Quantitative Anatomic Comparison of Microsurgical Transcranial, Endoscopic Endonasal, and Transorbital Approaches to the Orbit and Surrounding Skull-Base Regions

Edoardo Agosti, MD, PhD [1], Marco Valentini, MD[2], Karen Mapelli, MS[1], Ludovico Agostini, MD[3], Barbara Buffoli, PhD[4], Vittorio Rampinelli, MD, PhD[5], A. Yohan Alexander, MS[6,7,8], Maria Peris-Celda, MD, PhD[6,7,9], Marco Ravanelli, MD, PhD[10], Amedeo Piazza, MD[11], Pier Paolo Panciani, MD, PhD[1], Lena Hirtler, MD, PhD[12], Rita Rezzani, MD, PhD[4], Mario Turri-Zanoni, MD, PhD[2], Marco Maria Fontanella, MD[1], Francesco Doglietto, MD, PhD[3,13]

[1]Division of Neurosurgery, Department of Medical and Surgical Specialties, Radiological Sciences and Public Health, University of Brescia, Brescia, Italy; **(Continued on next page)**

Part of the results of this manuscript was presented at the North American Skull Base Society (NASBS) 35th Annual Meeting in San Diego, CA, on March 5-8, 2026.

Correspondence: Edoardo Agosti, MD, PhD, Division of Neurosurgery, Department of Medical and Surgical Specialties, Radiological Sciences and Public Health, University of Brescia, Piazza Spedali Civili, 1, Brescia 25123, Italy. Email: edoardo_agosti@libero.it

Received, February 10, 2026; **Accepted,** June 19, 2026; **Published Online,** September 25, 2026.

Operative Neurosurgery 00:1–17, 2026 https://doi.org/10.1227/ons.0000000000002166

© Congress of Neurological Surgeons 2026. All rights reserved.

BACKGROUND AND OBJECTIVE: Microsurgical transcranial approaches (MTAs) to the orbit and surrounding skull-base region lesions have been progressively complemented by endoscopic endonasal approaches (EEAs) and endoscopic transorbital approaches (ETOAs). This study provides the first quantitative, navigation-based comparison of working volumes and exposure areas of major approaches to the orbit and surrounding skull-base regions.

METHODS: Five alcohol-fixed specimens were dissected. Twenty-six subregions grouped into the orbit, midline, spheno-orbital, and cavernous regions were segmented. Nineteen approaches, including anterior MTAs, anterolateral MTAs, EEAs, and ETOAs, were performed. Exposure areas and working volumes were quantified.

RESULTS: Endoscopic endonasal transpterygoid approach (EETPA) provided the greatest exposure of the optic foramen (67.98%, $P = .03$ vs EEA to the medial orbit). The superior eyelid approach with lateral orbitotomy achieved the widest access to the lateral orbital wall, reaching 98.56% in the middle and 99.42% in the temporal portions ($P < .05$ vs the orbitozygomatic approach [OZA]). The transcaruncular approach better exposed medial wall (99.41%, $P = .04$ vs EETPA), and the inferolateral approach gained largest orbital floor exposure (99.18%, $P < .001$). The extended transbasal approach maximally exposed the planum sphenoidale (99.28%, $P = .03$ vs orbitozygomatic approach with anterior clinoidectomy [OZA + AC]), while the EETPA the chiasmatic sulcus and the tuberculum sellae (98.76% and 96.47%, $P < .001$). The OZA + AC dominated most subregions, including greater wing, optic canal roof, and superior orbital fissure (98.49%, 98.18%, and 98.68%, $P < .05$). The superior eyelid approach with lateral orbitotomy better exposed foramen ovale at 88.89% ($P < .01$), foramen rotundum at 88.78% ($P < .001$), intracranial V3 at 92.92% ($P = .04$), and petrous apex at 93.85% ($P < .01$), while OZA + AC maximized intracranial V1 and V2 (87.94% and 90.74%, $P < .05$). The MTAs had largest working volumes (extended transbasal approach 59.35 cm^3; OZA + AC 53.69 cm^3).

CONCLUSION: ETOAs provide unmatched access to the lateral orbit and cavernous regions, while EEAs excel medially and MTAs, especially OZA + AC, remain indispensable for broad spheno-orbital exposure and maximal working volumes.

KEY WORDS: Orbit, Skull base, Surgical approaches, Endoscopy, Microsurgery, Quantitative study

ABBREVIATIONS: BSFA, bilateral subfrontal approach; **CR,** cavernous region; **CSLW,** cavernous sinus lateral wall; **CSu,** chiasmatic sulcus; **EEAMO,** endoscopic endonasal approach to the medial orbit; **EEAs,** endoscopic endonasal approaches; **EETPA,** endoscopic endonasal transpterygoid approach; **ETBA,** extended transbasal approach; **ETOAs,** endoscopic transorbital approaches; **FOA,** fronto-orbital approach; **GW,** greater wing; **ILETOA,** inferolateral endoscopic transorbital approach; **MOZA,** mini-orbitozygomatic approach; **MPTA,** minipterional approach; **MR,** midline region; **MS,** maxillary strut; **MTAs,** microsurgical transcranial approaches; **OF,** optic foramen; **OLW,** orbit lateral wall; **OLWt,** orbit lateral wall (temporal fossa); **OR,** orbit region; **ORo,** orbital roof; **OZA + AC,** orbitozygomatic approach with anterior clinoidectomy; **OZA,** orbitozygomatic approach; **PA,** petrous apex; **PS,** planum sphenoidale; **PTA,** pterional approach; **SETOA + LO,** superior eyelid approach with lateral orbitotomy; **SETOA,** superior eyelid approach; **SOF,** superior orbital fissure; **SOR,** spheno-orbital region; **sSBRs,** surrounding skull-base regions; **TBA,** transbasal approach; **TCETOA,** transcaruncular endoscopic transorbital approach; **TFSA,** transfrontal sinus approach; **TS,** tuberculum sellae; **USFA,** unilateral subfrontal approach.

Supplemental digital content is available for this article at operativeneurosurgery-online.com.

© Congress of Neurological Surgeons 2026. Unauthorized reproduction of this article is prohibited.

The orbit and surrounding skull-base regions (sSBRs) represent a complex anatomic and surgical frontier at the intersection of neurosurgery, otolaryngology, and ophthalmology. These regions encompass intricate neurovascular structures including cranial nerves II to VI, along with the internal carotid artery and its branches.[1-4] Historically, these lesions were addressed by microsurgical transcranial approaches (MTAs), mainly variations of the pterional and subfrontal, which provided broad exposure through bony removal and cerebral retraction. In recent decades, the advent of endoscopic techniques has expanded the surgical armamentarium to include endoscopic endonasal approaches (EEAs) and endoscopic transorbital approaches (ETOAs), both offering more direct and potentially less invasive access to these regions.[5-10]

Despite increasing literature on the use of various open and endoscopic approaches to the orbit and sSBRs, indications for each are largely guided by surgeon and institution-specific preferences and experience. No study has clearly quantified the access provided to the orbit and sSBRs. In this study, we aim to quantitatively assess working volumes and exposure areas provided to various regions of the orbit and sSBRs through the main open and endoscopic approaches.

METHODS

Ethical Considerations

This work was performed according to the ethical standards of our Institutional Review Board. All human cadaveric studies have been performed in accordance with the ethical standards laid down in the 1964 Declaration of Helsinki and its later amendments. The article does not contain clinical studies or patient data.

Specimens

Five fresh-frozen adult human head specimens (10 sides) were used. Arterial vasculature was injected with red-colored silicone rubber (Xiameter® RTV, Dow Corning®) through the common carotids and vertebral arteries.[11-25]

CT Scan and Neuronavigation

High-resolution computed tomography (CT) was performed on each specimen using a 128-slice scanner (Somatom Definition Flash®, Siemens). The CT scan acquired from the vertex to the fifth cervical vertebra and reconstructed in 1-mm slices. The Digital Imaging and Communications in Medicine files were uploaded to a surgical navigation platform (GTx-Eyes II, University Health Network–University of Toronto) for real-time optical neuronavigation and 3-dimensional reconstructions.[11-28]

Surgical Approaches

All dissections were performed in a dedicated anatomic laboratory using standard microsurgical and endoscopic skull-base instrumentation. Microsurgical visualization was achieved using a Leica® M320 surgical microscope (Leica Microsystems), whereas endoscopic visualization was provided by a 4K endoscope system with 0° and 30° rigid scopes (Karl Storz®).[11] High-speed drills and craniotomes (Anspach®) were used.[11]

Nineteen surgical approaches (ie, 7 anterior MTAs, 6 anterolateral MTAs, 2 EEAs, and 4 ETOAs) were performed bilaterally on each specimen (Figure 1). The following anterior MTAs were quantified: supraorbital approach,[29] fronto-orbital approach (FOA),[29] unilateral subfrontal approach (USFA),[30] bilateral subfrontal approach (BSFA),[31] transfrontal sinus approach (TFSA),[32] transbasal approach (TBA),[33] and the extended transbasal approach (ETBA).[34] The following anterolateral MTAs were investigated: lateral supraorbital approach,[29] minipterional approach (MPTA),[35] pterional approach (PTA),[36] mini-orbitozygomatic approach (MOZA),[37] orbitozygomatic approach (OZA),[37] and orbitozygomatic approach with anterior clinoidectomy (OZA + AC).[37] The following EEAs were performed: endoscopic endonasal transpterygoid approach (EETPA),[38] and the endoscopic endonasal approach to the medial orbit (EEAMO).[34] The following ETOAs were performed: inferolateral endoscopic transorbital approach (ILETOA),[39] transcaruncular endoscopic transorbital approach (TCETOA),[40] superior eyelid approach (SETOA),[40] and the superior eyelid approach with lateral orbitotomy (SETOA + LO).[40]

All surgical approaches were performed in a modular, stepwise manner, progressing from less to more extensive, to preserve anatomic integrity and minimize overlap bias. The dissections were performed according to the sequence: supraorbital approach, FOA, USFA, BSFA, TFSA, TBA, lateral supraorbital approach, MPTA, PTA, EETPA, EEAMO, TCETOA, ILETOA, SETOA, SETOA + LO, MOZA, OZA, OZA + AC, and ETBA. Bone flaps were repositioned after each transcranial approach[11] to restore anatomy before dissections. Anterior clinoidectomy was performed only during the OZA to minimize corridor interference.

Surgical Corridor Quantification

An optical neuronavigation system (Polaris Vicra®; Northern Digital Inc.) coupled with GTx-Eyes II was used to quantify the maximum surgical volume with the highest surgical maneuverability (ie, "non-crossing" modality),[11] and the largest exposure obtained with straight instruments (ie, "crossing" modality; Figure 2).[11] Data collection was repeated 3 times for each modality. The deep surface of each surgical

(Continued from previous page)

[2]Division of Otorhinolaryngology, Department of Biotechnology and Life Sciences, University of Insubria, ASST Lariana, Como, Italy; [3]Neurosurgery, Fondazione Policlinico Universitario A. Gemelli IRCCS, Rome, Italy; [4]Department of Clinical and Experimental Sciences, Section of Anatomy and Physiopathology, University of Brescia, Brescia, Italy; [5]Unit of Otorhinolaryngology-Head and Neck Surgery, Department of Surgical Specialties, Radiological Sciences and Public Health, University of Brescia, Brescia, Italy; [6]Rhoton Neurosurgery and Otolaryngology Surgical Anatomy Program, Mayo Clinic, Rochester, Minnesota, USA; [7]Department of Neurologic Surgery, Mayo Clinic, Rochester, Minnesota, USA; [8]Medical School, University of Minnesota, Minneapolis, Minnesota, USA; [9]Department of Otolaryngology/Head and Neck Surgery, Mayo Clinic, Rochester, Minnesota, USA; [10]Radiology Unit, Department of Medical and Surgical Specialties, Radiological Sciences and Public Health, University of Brescia, Spedali Civili, Brescia, Italy; [11]Division of Neurosurgery, Department of Neuroscience, "Sapienza" University of Rome, Rome, Italy; [12]Center for Anatomy and Cell Biology, Division of Anatomy, Medical University of Vienna, Vienna, Austria; [13]Department of Neurosurgery, Università Cattolica del Sacro Cuore, Rome, Italy

© Congress of Neurological Surgeons 2026. Unauthorized reproduction of this article is prohibited.

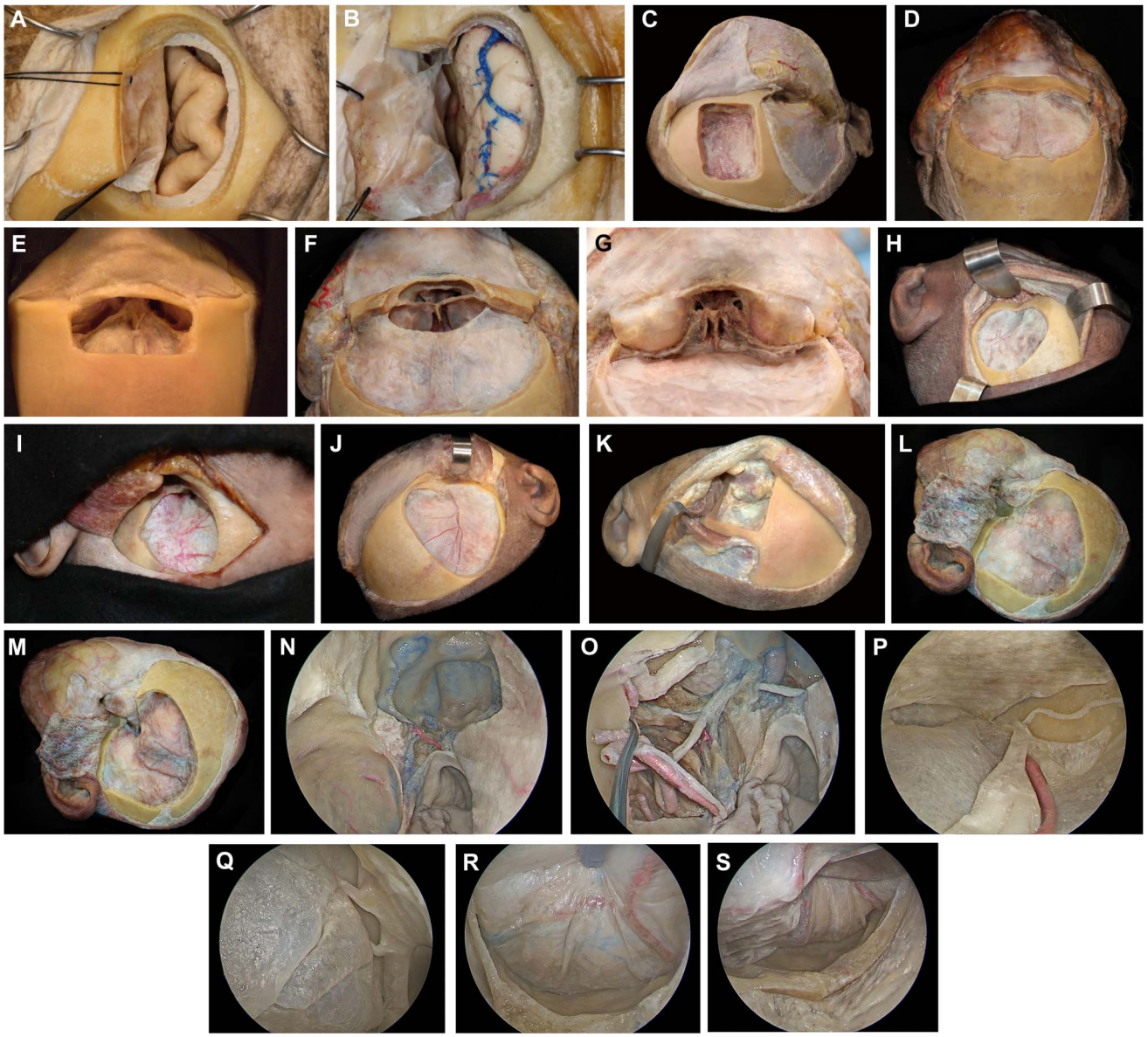


FIGURE 1. *Nineteen surgical approaches (7 anterior microsurgical transcranial approaches, 6 anterolateral microsurgical transcranial approaches, 2 endoscopic endonasal approaches, and 4 endoscopic transorbital approaches) were performed bilaterally on each specimen.* **A**, *Supraorbital approach;* **B**, *fronto-orbital approach;* **C**, *unilateral subfrontal approach;* **D**, *bilateral subfrontal approach;* **E**, *transfrontal sinus approach;* **F**, *transbasal approach;* **G**, *extended transbasal approach;* **H**, *lateral supraorbital approach;* **I**, *minipterional approach;* **J**, *pterional approach;* **K**, *mini-orbitozygomatic approach;* **L**, *orbitozygomatic approach;* **M**, *orbitozygomatic approach with anterior clinoidectomy;* **N**, *endoscopic endonasal approach to the medial orbit;* **O**, *endoscopic endonasal transpterygoid approach;* **P**, *inferolateral endoscopic transorbital approach;* **Q**, *transcaruncular endoscopic transorbital approach;* **R**, *superior eyelid approach;* **S**, *superior eyelid approach with lateral orbitotomy.*

pyramid was traced during the dissection using a calibrated pointer, and the superficial surface was automatically calculated based on standardized tool lengths. The height of the surgical corridor was set at the level of the craniotomy for MTAs, of the nasal pyriform aperture for EEA, and of the orbital rim for ETOAs. Exposure areas and working volumes were computed in real time and reviewed on axial, coronal, sagittal, and 3-dimensional planes.

During MTAs surgical corridor quantifications, frontal and temporal lobes retraction was kept constant to 15 mm with the aid of a Greenberg® Retractor System.

© Congress of Neurological Surgeons 2026. Unauthorized reproduction of this article is prohibited.

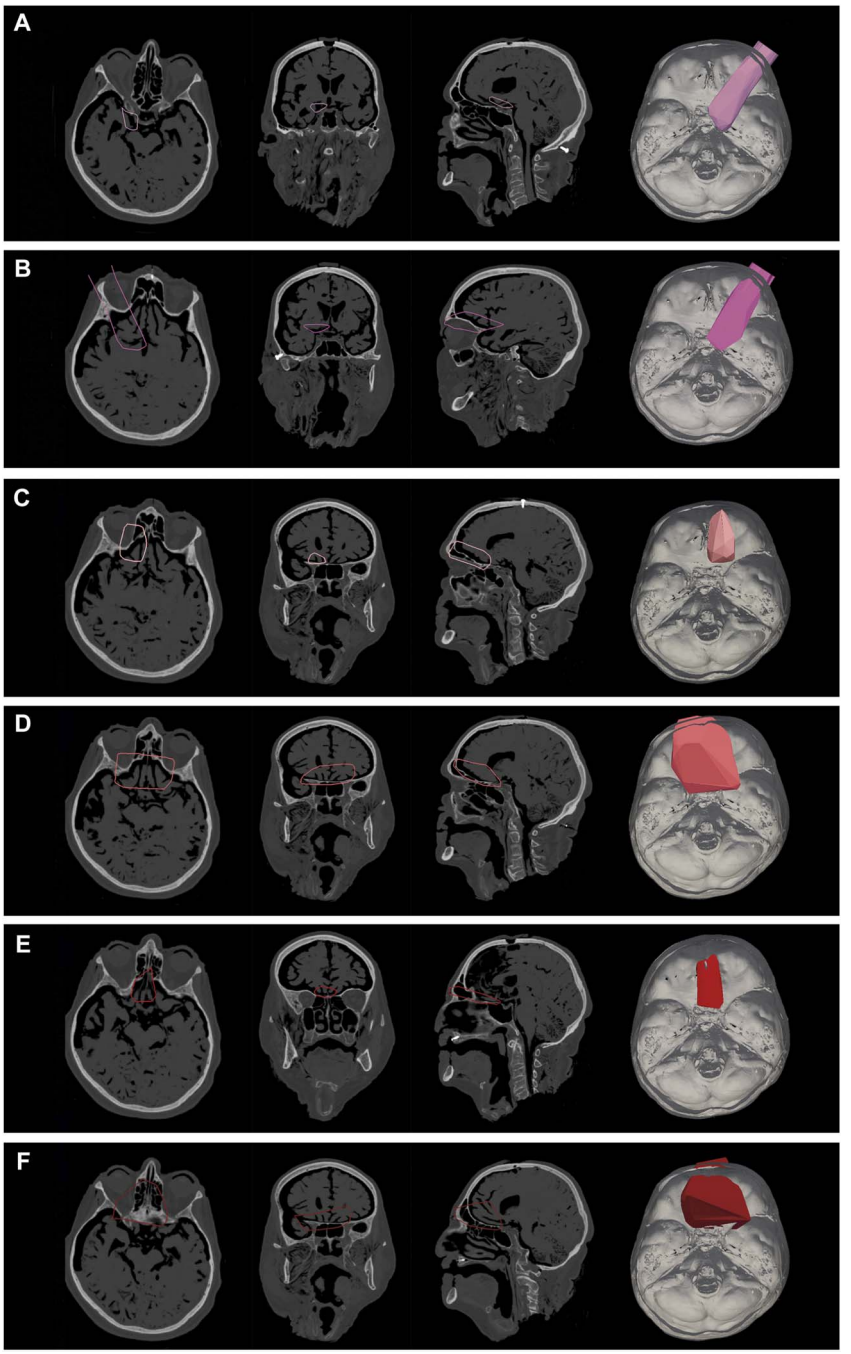


FIGURE 2. *Screenshots from ApproachViewer in axial, coronal, and sagittal planes and 3-dimensional volume rendering of quantified noncrossing anterior microsurgical transcranial approaches, anterolateral microsurgical transcranial approaches, endoscopic endonasal approaches, and endoscopic transorbital approaches.* **A**, *Supraorbital approach;* **B**, *fronto-orbital approach;* **C**, *unilateral subfrontal approach;* **D**, *bilateral subfrontal approach;* **E**, *transfrontal sinus approach;* **F**, *transbasal approach;* **G**, *extended transbasal approach;* **H**, *endoscopic endonasal approach to the medial orbit;* **I**, *endoscopic endonasal transpterygoid approach;* **J**, *lateral supraorbital approach;* **K**, *minipterional approach;* **L**, *pterional approach;* **M**, *mini-orbitozygomatic approach;* **N**, *orbitozygomatic approach;* **O**, *orbitozygomatic approach with anterior clinoidectomy;* **P**, *inferolateral approach;* **Q**, *transcaruncular approach;* **R**, *superior eyelid approach;* **S**, *superior eyelid approach with lateral orbitotomy.*

© Congress of Neurological Surgeons 2026. Unauthorized reproduction of this article is prohibited.

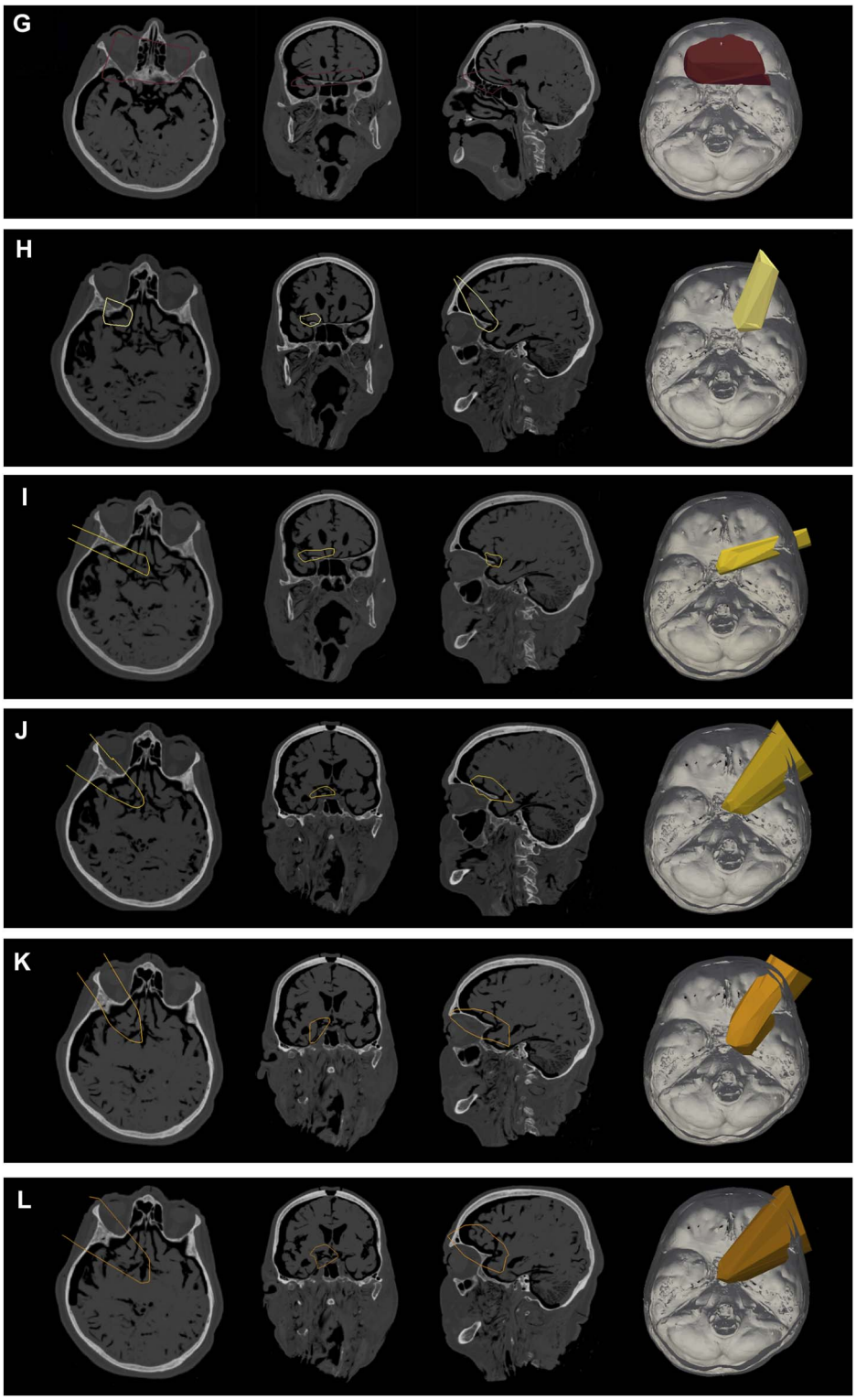


FIGURE 2. *Continued.*

© Congress of Neurological Surgeons 2026. Unauthorized reproduction of this article is prohibited.

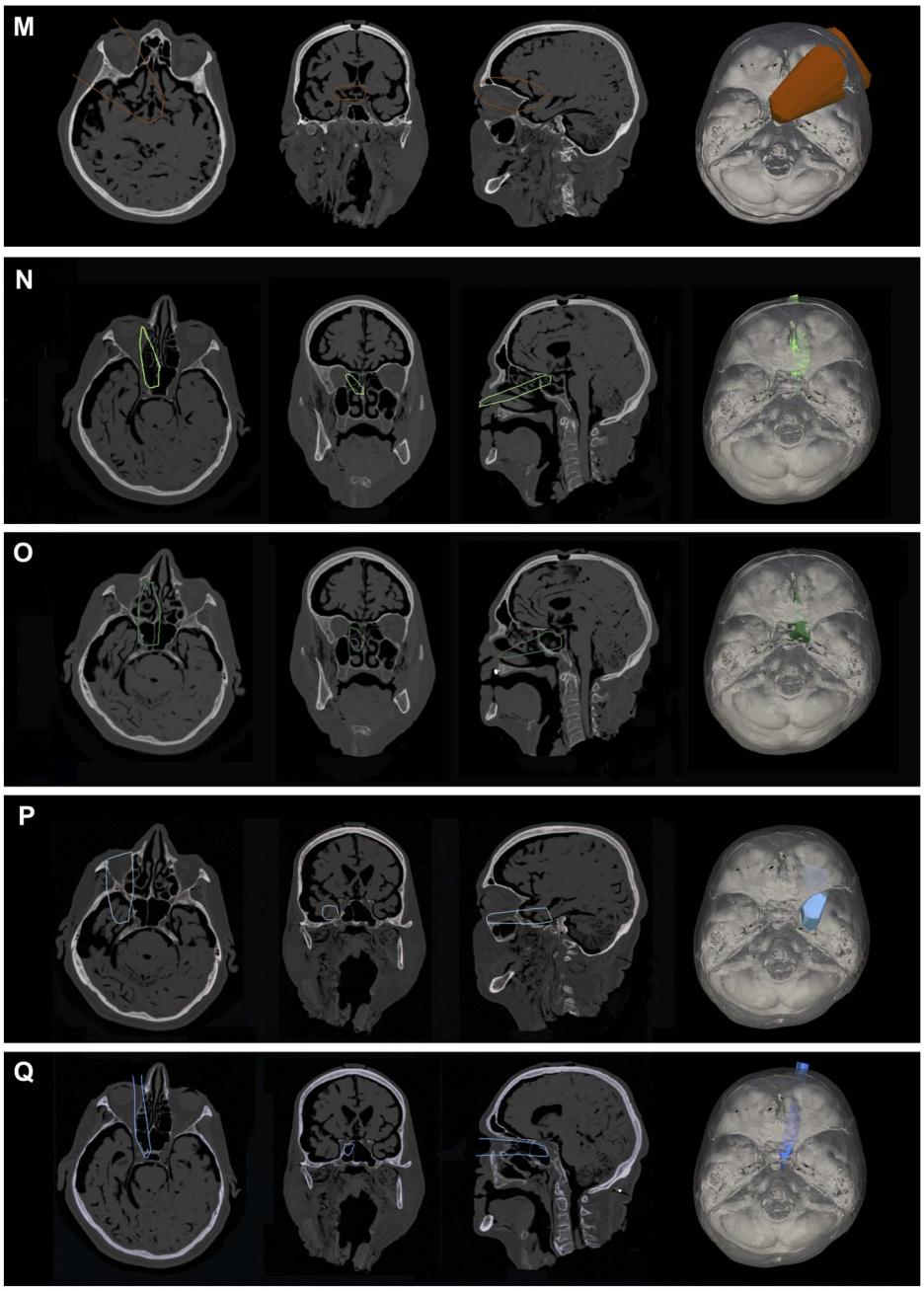


FIGURE 2. *Continued.*

Surface Rendering and Quantification of Exposed Area

The orbit and sSBRs were segmented into 26 anatomic subregions (Figure 3), further grouped into 4 macro-regions: orbit region (OR), composed by the orbital roof (ORo), orbit lateral wall (temporal fossa) (OLWt), orbit lateral wall (middle cranial fossa), orbital floor, orbit medial wall, and optic foramen (OF); midline region (MR), divided in planum sphenoidale (PS), sphenoid limbus, chiasmatic sulcus (CSu), and tuberculum sellae (TS); spheno-orbital region (SOR), composed by greater wing (GW), lesser wing, anterior clinoid process, optic canal roof, optic strut, superior orbital fissure, sagittal crest, and maxillary strut (MS); and cavernous region (CR), divided in foramen ovale, foramen rotundum, cavernous sinus lateral wall, intracranial V1, intracranial V2,

© Congress of Neurological Surgeons 2026. Unauthorized reproduction of this article is prohibited.

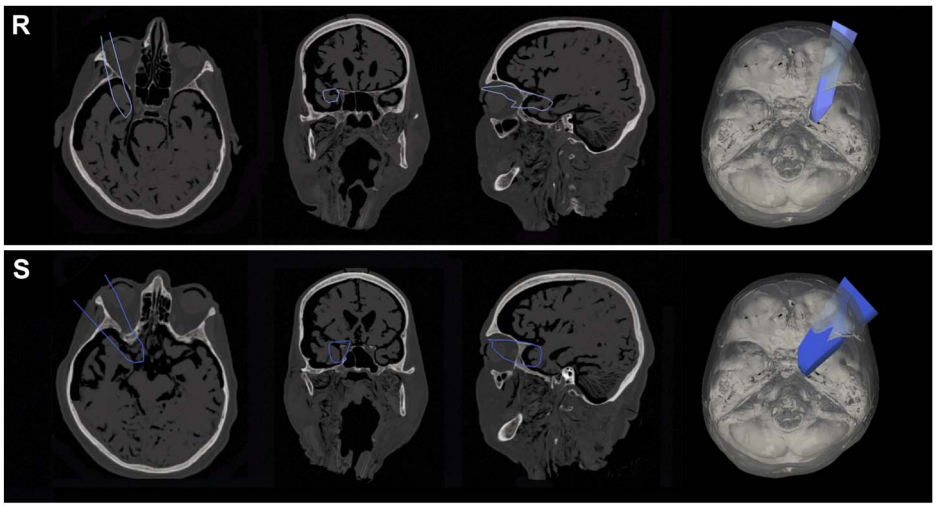


FIGURE 2. *Continued.*

intracranial V3, gasserian ganglion, and petrous apex (PA). Three-dimensional surface rendering and segmentation were performed on CT data sets using Insight Toolkit SNAP software (version 4.2.2, www.itksnap.org), with each surface saved as .mha and .stl files for analysis. Dedicated software (Autodesk Meshmixer 3.5® and ApproachViewer, part of GTX-Eyes-II)[26] quantified the percentage value of exposed area by all approaches for each of the 26 surfaces.

Statistical Analysis

All values were recorded and processed using Microsoft Excel (Microsoft Corporation). Statistical analysis was performed using linear mixed models with random intercepts for each specimen to account for intrasample variability. Exposure area and working volume were compared across approaches. Statistical significance was set at $P < .05$, and confidence intervals were estimated using bootstrap resampling (1000 iterations). Data processing was conducted using STATA® (StataCorp LLC).

RESULTS

A total of 29 640 measurements were obtained from 19 approaches and 26 anatomic subregions. Each approach contributed 60 measurements across 5 specimens, bilateral analysis, crossing and noncrossing modalities, and 3 repetitions per modality. The mean percentages of exposed orbit and sSBR areas by each surgical approach are reported in detail in **Supplemental Digital Content 1**, **Tables 1-26**, https://links.lww.com/ONS/B350 and graphically summarized in Figures 4-6. Small statistically significant differences likely reflect interspecimen variability.

Areas of Exposure

Orbit Region

The OF was maximally exposed by the EETPA (67.98%), which provided significantly more exposure than EEAMO (54.92%, $P = .03$) and OZA + AC (40.11%, $P = .01$). Among ETOAs, SETOA + LO provided the most exposure to OF (40.11%), whereas TCETOA yielded the least (9.67%).

For the orbit lateral wall (middle cranial fossa), SETOA + LO achieved the greatest exposure (98.56%), followed closely by SETOA (96.87%), both significantly surpassing OZA (93.99%, $P = .04$). For the OLWt, the most exposure was provided by SETOA + LO (99.42%). This was significantly more exposure than OZA (91.72%, $P = .02$) and MOZA (55.48%, $P = .01$). SETOA achieved 98.66% of the OLWt, whereas EEA-based techniques were noncontributory for the OLW.

The orbit medial wall was primarily accessible through EEAs and ETOAs. TCETOA provided near-complete exposure (99.41%), significantly outperforming EETPA (90.25%, $P = .04$) and EEAMO (83.01%, $P = .01$). Conversely, MTAs afforded no exposure to this subregion.

For the orbital floor, ILETOA offered the most extensive access (99.18%), with a significant advantage over SETOA (39.44, $P < .001$) and EEAMO (25.63%, $P < .001$). Intermediate exposures were provided by TCETOA (38.76%) and SETOA + LO (39.44%).

The ORo was best addressed by MTAs, where OZA + AC achieved the maximum exposure, significantly exceeding TBA (99.21% vs 95.88%, $P = .04$). Among less extensive MTAs, FOA exposed 92.17%, whereas the best-performing ETOA was the SETOA + LO at 67.90% (Figure 4, **Supplemental Digital Content 1**, **Tables 1-6**, https://links.lww.com/ONS/B350).

Midline Region

Exposure of the MR demonstrated a clear predominance of MTAs and EEAs, with significant variability across its subregions. The PS was most extensively exposed by ETBA (99.28%), with a minimal but statistically significant advantage of 2.02% compared with OZA

© Congress of Neurological Surgeons 2026. Unauthorized reproduction of this article is prohibited.

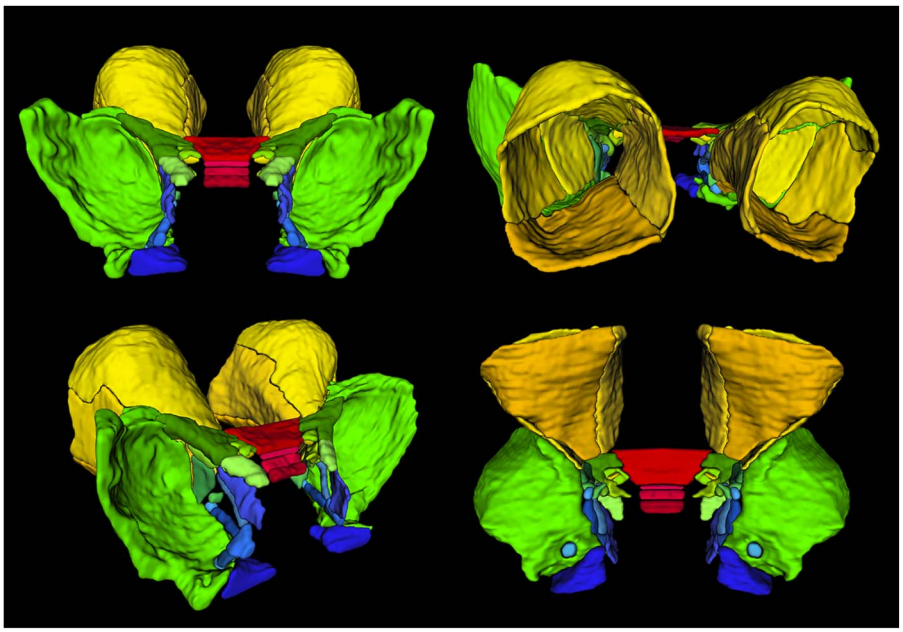


FIGURE 3. *Three-dimensional volume rendering of the orbit and surrounding skull base region surfaces drawn bilaterally, shown with an intracranial perspective. The orbit and surrounding skull-base regions were divided in 26 target areas, drawn on each computed tomography and grouped in 4 macro-regions. (1) Orbit region: 1. orbital roof: situated behind the supraorbital margin and forms the roof of the orbits; 2. orbit lateral wall (temporal fossa): composed by the zygomatic bone anteriorly and the greater wing of the sphenoid bone posteriorly; 3. orbit lateral wall (middle cranial fossa): formed by the greater wing of the sphenoid bone; 4. orbital floor: inferior wall made up of the orbital surfaces of the maxilla and zygomatic bones; 5. orbit medial wall: built out of the maxilla, the lacrimal bone, the orbital plate of the ethmoid bone, and the LW of the sphenoid bone; 6. optic foramen: cylindrical canal running obliquely through the LW of sphenoid bone that transmits the optic nerve and ophthalmic artery. (2) Midline region: 1. planum sphenoidale: anterior portion of the sphenoid bone extended from the ethmoidal arteries to the posterior margin of the chiasmatic sulcus (limbus sphenoidale) and bound laterally by the medial part of the orbital roofs; 2. sphenoid limb: prominent ridge on the body of the sphenoid bone forming the posterior border of the jugum sphenoidale and the anterior border of the prechiasmatic sulcus; 3. chiasmatic sulcus: groove on the superior surface of the sphenoid bone and at each lateral end are located the optic canals; 4. tuberculum sellae: bony elevation ridge that extends from the limbus sphenoidale to the superior margin of the sellae turcica. (3) Spheno-orbital region: 1. greater wing: bony process that projects laterally to the sphenoid body bounded by the sphenosquamosal suture and petrous bone anteriorly, the temporoparietal suture laterally, the lateral wall of the cavernous sinus medially, and SOF anteriorly; 2. LW: bony structure that continues laterally from the ACP up to the sphenosquamosal suture, delimited anteriorly by the frontosphenoidal suture and posteriorly by the sphenoid ridge; 3. ACP: bony projection extending from the LW of the sphenoid bone, forming a part of the lateral wall of the optic canal; 4. optic canal roof: superior bony wall of the optic canal in the LW of the sphenoid bone; 5. optic strut: joins the body of the sphenoid bone with the ACP, and separates the optic canal superomedially from the SOF inferomedially; 6. SOF: space located at the orbital apex with an anterolateral course, bounded by the greater wing, LW, and body of sphenoid; 7. sagittal crest: bone ridge triangle shaping dorsally the SOF; 8. maxillary strut: bone that separates the FR and SOF. (4) Cavernous region: 1. foramen ovale: posterolateral to the FR and lateral to the lingula of the sphenoid bone, through this the mandibular nerve enters the skull; 2. FR: circular hole in the sphenoid bone located at the base of greater wing, inferomedially to the SOF; 3. cavernous sinus lateral wall: extending from the SOF anteriorly to the apex of the petrous temporal bone posteriorly; 4. intracranial V1: ophthalmic branch of trigeminal nerve who emerges through the SOF; 5. intracranial V2: maxillary branch of trigeminal nerve who emerges through the FR; 6: intracranial V3: mandibular branch of trigeminal nerve who emerges through the foramen ovale; 7. gasserian ganglion: sensory ganglion of the trigeminal nerve located in the Meckel cave, near the apex of the petrous part of the temporal bone; 8. petrous apex: the surface extending from the Kawase triangle laterally to the most medial part of the petrous bone. ACP, anterior clinoid process; FR, foramen rotundum; LW, lesser wing; SOF, superior orbital fissure.*

© Congress of Neurological Surgeons 2026. Unauthorized reproduction of this article is prohibited.

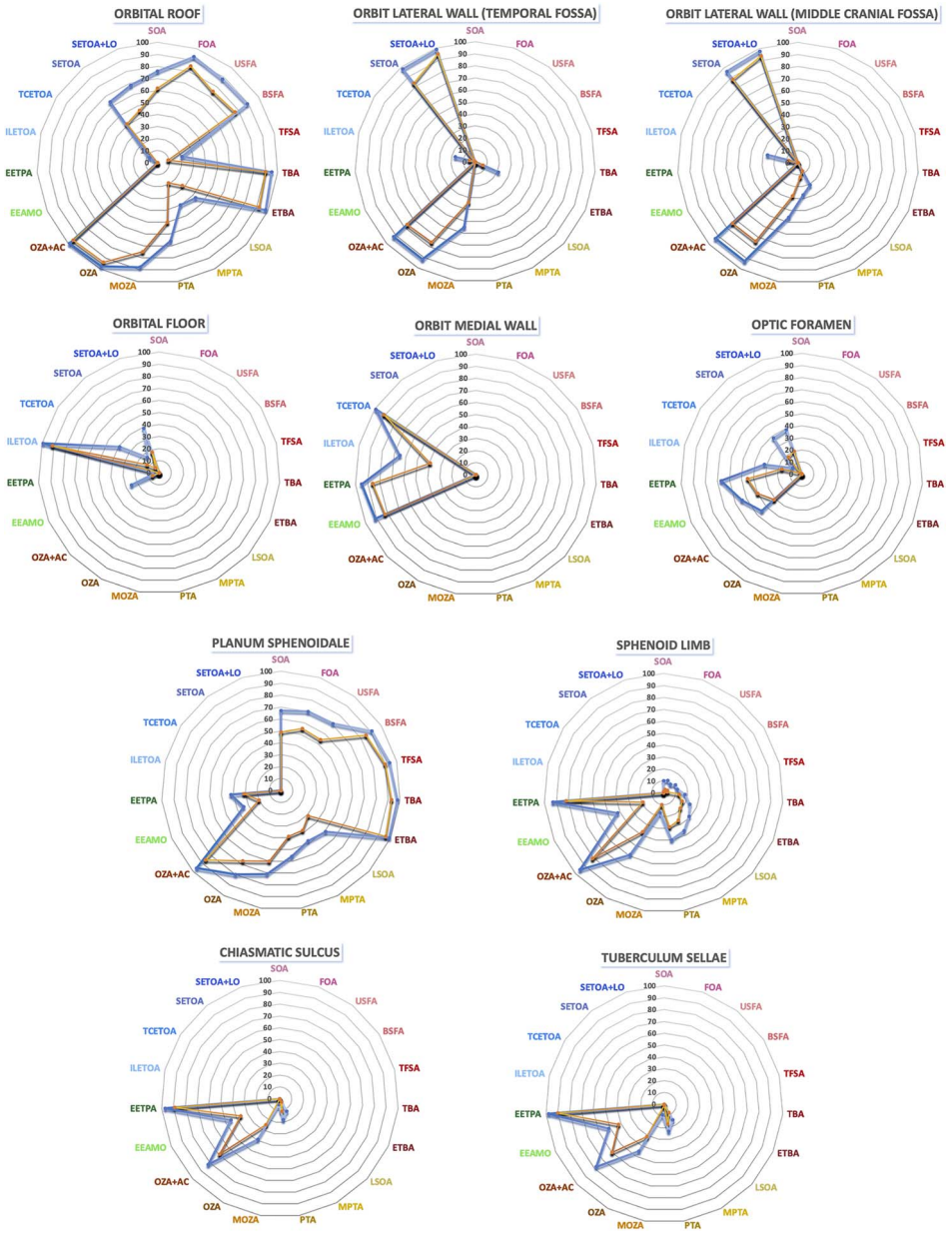


FIGURE 4. *Exposure of the orbit region and midline region offered by all studied approaches. The radar diagrams show the percentage value of exposed area obtained by each approach for each surface, as measured in noncrossing (orange) and crossing (blue) modalities. Approaches are sorted clockwise and grouped in anterior microsurgical transcranial approaches, anterolateral microsurgical transcranial approaches, endoscopic endonasal approaches, and endoscopic transorbital approaches. BSFA, bilateral subfrontal approach; EEAMO, endoscopic endonasal approach to the medial orbit; EETPA, endoscopic endonasal transpterygoid approach; ETBA, extended transbasal approach; FOA, fronto-orbital approach; ILETOA, inferolateral approach; LSOA, lateral supraorbital approach; MOZA, mini-orbitozygomatic approach; MPTA, minipterional approach; OZA, orbitozygomatic approach; OZA + AC orbitozygomatic approach with anterior clinoidectomy; PTA, pterional approach; SETOA, superior eyelid approach; SETOA + LO, superior eyelid approach with lateral orbitotomy; SOA, supraorbital approach; TBA, transbasal approach; TCETOA, transcaruncular approach; TFSA, transfrontal sinus approach; USFA, unilateral subfrontal approach.*

© Congress of Neurological Surgeons 2026. Unauthorized reproduction of this article is prohibited.

+ AC (P = .03). Among anterior MTAs to the PS, TFSA (94.88%) and BSFA provided the most exposure (91.56%). Endonasal corridors yielded modest exposures, with EETPA achieving significantly less exposure than ETBA (99.28% vs 56.67%, P < .001).

For the sphenoid limbus, OZA + AC provided the most exposure, minimally outperforming EETPA by (95.66% vs 93.83%), but offering an exposure gain of 77.40% over PTA (P < .001) and 81.40% over BSFA (P < .001).

EETPA offered the most exposure of the CSu (96.47%), which was significantly more than OZA + AC (80.55%, P < .001) and EEAMO (44.22%, P < .001). Among MTAs, only OZA + AC provided relevant exposure (81.55%).

For the TS, EETPA provided near-complete exposure, significantly surpassing EEAMO (98.76% vs 51.92%, P < .001) and OZA + AC (98.76% vs 78.67%, P = .01) (Figure 4, **Supplemental Digital Content 1**, **Tables 7-10**, https://links.lww.com/ONS/B350). Overall, findings represent differences in surgical corridor geometry rather than clinical applicability and should be interpreted as quantitative measures of access rather than surgical superiority. As cadaveric data, clinical applicability remains limited.

Spheno-Orbital Region

Exposure of the SOR was best achieved with OZAs, particularly OZA + AC. The GW was most extensively exposed through OZA + AC (98.76%). This was significantly more than MOZA (60.44%, P < .001). No endonasal route achieved measurable exposure of this region.

For the lesser wing, OZA + AC maintained superiority (89.12%), exceeding OZA (88.47%, P = .22) and MOZA (71.02%, P < .05). Anterior MTAs offered modest crossing coverage of the region (33.53%-69.91%).

The anterior clinoid process demonstrated the greatest benefit from anterior clinoidectomy: OZA + AC achieved significantly more exposure than MOZA (89.11% vs 70.98%, P < .05).

The optic canal roof followed a similar trend, with OZA + AC significantly surpassing the exposure of MOZA (98.18% vs 94.11%, P = .05). The optic strut was primarily exposed by OZA + AC (72.14%), which provided a significant advantage over MOZA (53.76%, P < .05) and SETOA + LO (25.88, P < .001).

For the superior orbital fissure, OZA + AC achieved significantly more access than MOZA (98.68% vs 46.29%, P < .001). For the MS, OZA + AC provided the highest exposure (95.12%), outperforming both PTA (78.37%, P < .001) and EETPA (79.36%, P < .001). Moreover, SETOA (89.07%, P < .01) and SETOA + LO (91.26%, P < .01) offered lower exposure of the MS compared with OZA + AC (Figure 5, **Supplemental Digital Content 1**, **Tables 11-18**, https://links.lww.com/ONS/B350). Notably, OZA + AC and SETOA + LO showed similarly high MS exposure, both exceeding PTA and EETPA, suggesting comparable functional access despite different routes. These findings should be interpreted within a macroregional framework, as corridors target broader regions rather than isolated structures. The same applies to CR, where differences reflect regional exposure patterns.

Cavernous Region

Anterolateral MTAs and ETOAs provided the most exposure to the CR. The foramen ovale was most extensively exposed through SETOA + LO, significantly surpassing OZA + AC (88.89 vs 69.29%, P < .01). OZA (51.85%) and PTA (20.99%) offered moderate-to-limited coverage.

For the foramen rotundum, SETOA + LO achieved maximal exposure (88.78%), exceeding SETOA (78.55%, P < .01) and OZA + AC (61.66%, P < .001).

The cavernous sinus lateral wall was best accessed by SETOA + LO (94.66%), which was slightly higher than SETOA (91.05%, P = .09) and OZA + AC (91.26%, P = .1). OZA offered significantly more access the PTA (79.37% vs 60.66%, P < .01). MPTA (19.59%) and EETPA (15.43%) provided limited exposure of the CSLW.

Intracranial V1 was primarily exposed through OZA + AC (87.94%), exceeding the SETOA (78.46%, P < .05) and SETOA + LO (78.69%, P < .05). Intracranial V2 exposure was highest with OZA + AC, which was significantly greater than the exposure with SETOA (90.74% vs 80.45%, P < .05). PTA offered significantly more exposure than MPTA (60.73% vs 31.88%, P < .01). Intracranial V3 was maximally exposed by SETOA + LO, which was significantly greater than the exposure afforded by OZA + AC (92.92% vs 85.71%, P = .04). PTA offered significantly more access than MPTA (92.92% vs 50.78%, P < .05).

Maximal exposure of the gasserian ganglion was afforded through SETOA + LO, which was significantly more than ILETOA (91. 64% vs 37.94%, P < .001). PTA offered significantly more access than MPTA (38.92% vs 8.18% P < .001). Finally, the PA was best visualized through SETOA + LO, which was slightly higher than SETOA (93.85 vs 78.75%, P < .01) (Figure 6, **Supplemental Digital Content 1**, **Tables 19-26**, https://links.lww.com/ONS/B350).

Approach Volumes

The MTAs working volume tended to increase with the invasiveness of the surgical approach, depending on the distance from the target (approximately 9 cm for USFA and BSFA, and around 10 cm for the other anterior and anterolateral MTAs). Among these, ETBA had the largest working volume (59.35 cm^3), followed by TBA (55.16 cm^3) and OZA combined with AC (53.69 cm^3). By contrast, EEAs and ETOAs had an average target distance of about 11 cm. Within EEAs, the working volumes were relatively similar (EETPA: 49.95 cm^3; EEAMO: 45.78 cm^3), both exceeding those of ETOAs (Figure 7, **Supplemental Digital Content 1**, **Table 27**, https://links.lww.com/ONS/B350).

DISCUSSION

In this study, we showed that (1) MTAs, especially ETBA and OZA + AC remain the gold standard for broad SOR exposure and maximal working volumes; (2) EEAs achieve unmatched access to

© Congress of Neurological Surgeons 2026. Unauthorized reproduction of this article is prohibited.

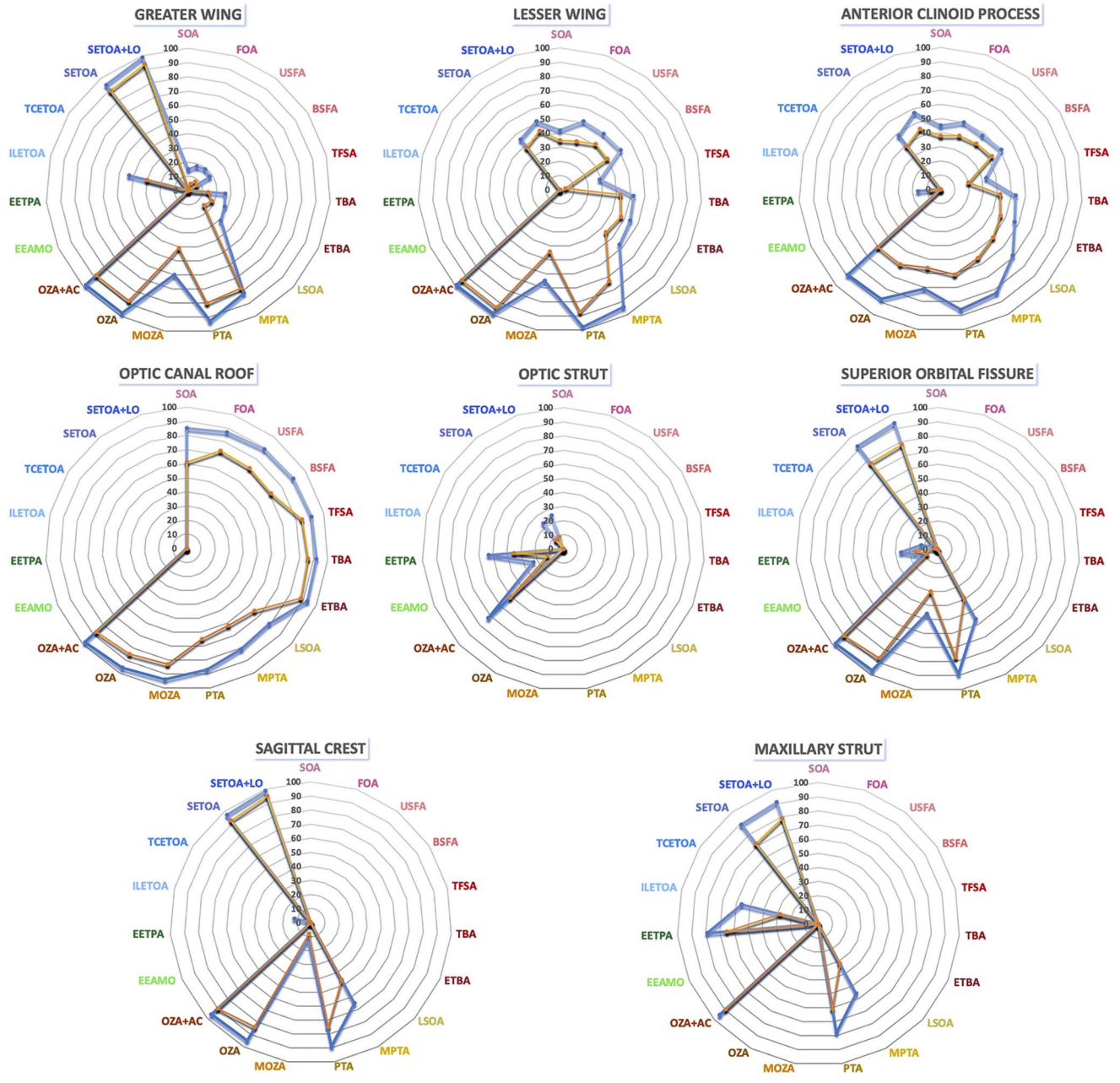


FIGURE 5. *Exposure of the SOR offered by all approaches studied. The radar diagrams show the percentage value of exposed area obtained by each approach for each surface, as measured in noncrossing (orange) and crossing (blue) modalities. Approaches are sorted clockwise and grouped in anterior microsurgical transcranial approaches, anterolateral microsurgical transcranial approaches, endoscopic endonasal approaches, and endoscopic transorbital approaches. BSFA, bilateral subfrontal approach; EEAMO, endoscopic endonasal approach to the medial orbit; EETPA, endoscopic endonasal transpterygoid approach; ETBA, extended transbasal approach; FOA, fronto-orbital approach; ILETOA, inferolateral approach; LSOA, lateral supraorbital approach; MOZA, mini-orbitozygomatic approach; MPTA, minipterional approach; OZA, orbitozygomatic approach; OZA + AC orbitozygomatic approach with anterior clinoidectomy; PTA, pterional approach; SETOA, superior eyelid approach; SETOA + LO, superior eyelid approach with lateral orbitotomy; SOA, supraorbital approach; SOR, spheno-orbital region; TBA, transbasal approach; TCETOA, transcaruncular approach; TFSA, transfrontal sinus approach; USFA, unilateral subfrontal approach.*

© Congress of Neurological Surgeons 2026. Unauthorized reproduction of this article is prohibited.

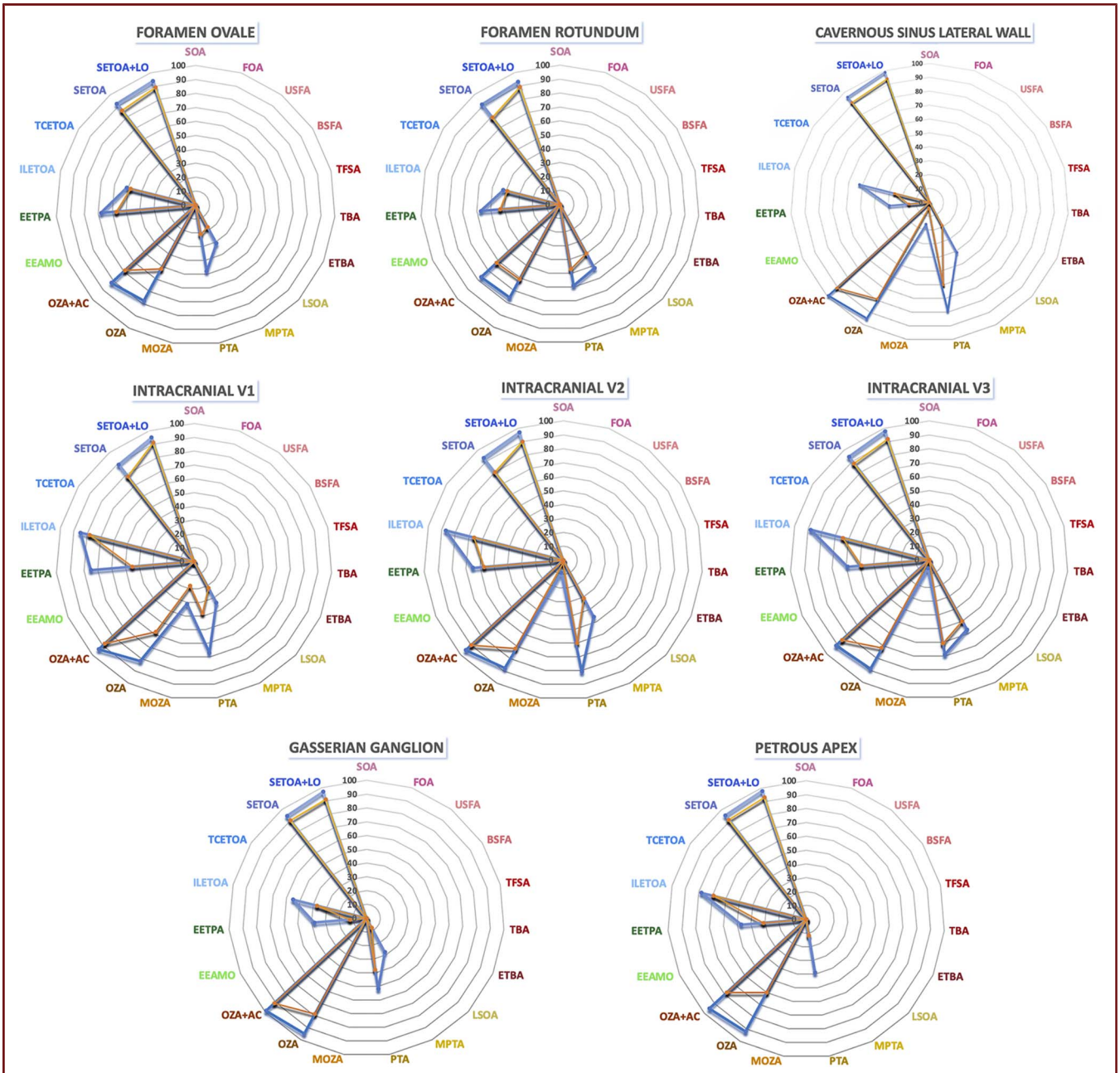


FIGURE 6. *Exposure of the cavernous region offered by all approaches studied. The radar diagrams show the percentage value of exposed area obtained by each approach for each surface, as measured in noncrossing (orange) and crossing (blue) modalities. Approaches are sorted clockwise and grouped in anterior microsurgical transcranial approaches, anterolateral microsurgical transcranial approaches, endoscopic endonasal approaches, and endoscopic transorbital approaches. BSFA, bilateral subfrontal approach; EEAMO, endoscopic endonasal approach to the medial orbit; EETPA, endoscopic endonasal transpterygoid approach; ETBA, extended transbasal approach; FOA, fronto-orbital approach; ILETOA, inferolateral approach; LSOA, lateral supraorbital approach; MOZA, mini-orbitozygomatic approach; MPTA, minipterional approach; OZA, orbitozygomatic approach; OZA + AC orbitozygomatic approach with anterior clinoidectomy; PTA, pterional approach; SETOA, superior eyelid approach; SETOA + LO, superior eyelid approach with lateral orbitotomy; SOA, supraorbital approach; TBA, transbasal approach; TCETOA, transcaruncular approach; TFSA, transfrontal sinus approach; USFA, unilateral subfrontal approach.*

© Congress of Neurological Surgeons 2026. Unauthorized reproduction of this article is prohibited.

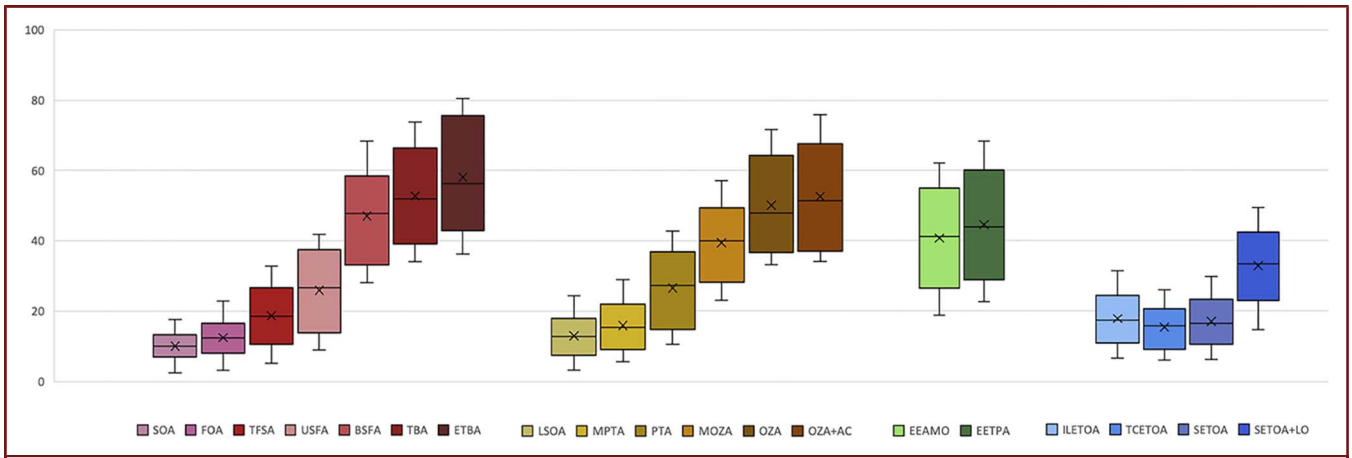


FIGURE 7. *Analysis of surgical volume provided by the different approaches studied. Boxplot representation of anterior microsurgical transcranial approaches, anterolateral microsurgical transcranial approaches, endoscopic endonasal approaches, and endoscopic transorbital approaches. Each boxplot indicates minimum, first quartile, median (middle bar), mean (cross), fourth quartile, and maximum values of each surgical volume. Volumetric values are expressed in cm^3. BSFA, bilateral subfrontal approach; EEAMO, endoscopic endonasal approach to the medial orbit; EETPA, endoscopic endonasal transpterygoid approach; ETBA, extended transbasal approach; FOA, fronto-orbital approach; ILETOA, inferolateral approach; LSOA, lateral supraorbital approach; MOZA, mini-orbitozygomatic approach; MPTA, minipterional approach; OZA, orbitozygomatic approach; OZA + AC orbitozygomatic approach with anterior clinoidectomy; PTA, pterional approach; SETOA, superior eyelid approach; SETOA + LO, superior eyelid approach with lateral orbitotomy; SOA, supraorbital approach; TBA, transbasal approach; TCETOA, transcaruncular approach; TFSA, transfrontal sinus approach; USFA, unilateral subfrontal approach.*

MR, such as the TS and CSu; (3) and ETOAs, particularly SETOA with or without lateral orbitotomy (SETOA ± LO), excel in lateral orbital and CR targets, complementing rather than replacing transcranial corridors.

Key findings include greater exposure, anatomic features, confirmation of previously reported findings in the literature,[11,40] and potential clinical relevance, particularly for ETOAs in spheno-orbital and CRs.

Access to several of the orbital regions and sSBRs is largely dictated by surgeon- and institution-specific preferences. As such, this study largely aims to provide objective data where ambiguity exists.[5,7,41] Regarding MR, MTAs and EEAs offered maximal and similar exposure.[6,42] The TS and CSu, however, were better exposed by EEAs.[6,42] For approaches to the CR, MTAs and ETOAs provided excellent access.[41] However, several advantages of SETOA ± LO must be acknowledged. First, SETOA ± LO provides direct access to the lateral wall of cavernous sinus and PA with minimal manipulation of the brain.[5,7] This is due both to the direct access SETOA ± LO provides to the CR once the GW has been drilled and the low-profile nature of the approach, as it uses the endoscope to access all parts of the sub-pretemporal corridors.[41]

Attention should be paid to the advantage provided by the LO as an adjunct to SETOA. The LO is specifically useful to provide medial access in the paramedian skull base (ie, CR and medial SOR), as surgical trajectory afforded is increasingly lateral to medial. The LO also affords subjectively easier dissection, as instruments are not confined by the bony limits of the orbit.[5,7]

Within the SOR, anterolateral MTAs remain the most comprehensive, providing wide, en face exposure of this region. The ETOAs better expose medial landmarks (ie, sagittal crest), especially when combined with LO. This suggests that, for selected lesions, transorbital strategies can rival traditional transcranial corridors, potentially reducing morbidity.[8,43]

The different regions of the OR were all best exposed by different approaches, as the orbits' various surfaces interface with distinct anatomic areas. The OMW and OF were best approached with TCETOA and ILETOA, respectively.[44] While EEAs afford less access to the full OF and OMW, they may offer easier access to multiple compartments and easier bimanual dissection. For the orbit lateral wall (OLW) and OR, ETOAs were effective at accessing the bone and may be excellent options in the setting of osseous lesions, including hyperostotic sphenoid wing meningiomas or fibrous dysplasia.[5,41,45] Furthermore, though ETOAs can access intradural compartments of lesions as well, they may not be ideal for lesions that extend superiorly and laterally, as the impediment of the globe restricts this operative trajectory. In addition, if lesions include hyperostosis of the frontotemporal craniectomy, an MTA is ideal to access this portion of the lesion and reconstruct the bone for cosmetic purposes. So, MTAs may be best to fully address lesions in multiple compartments of the skull base.

When comparing this study with the main previously published literature, our results largely reinforce many of the subjective/didactic data with objective data. Perneczky et al[29] and Figueiredo et al[35] documented the incremental gains from MPTA to OZA; we provided quantitative confirmation across 26 subregions. Similarly, Locatelli et al[40] demonstrated the feasibility of SETOA and TCETOA to the

© Congress of Neurological Surgeons 2026. Unauthorized reproduction of this article is prohibited.

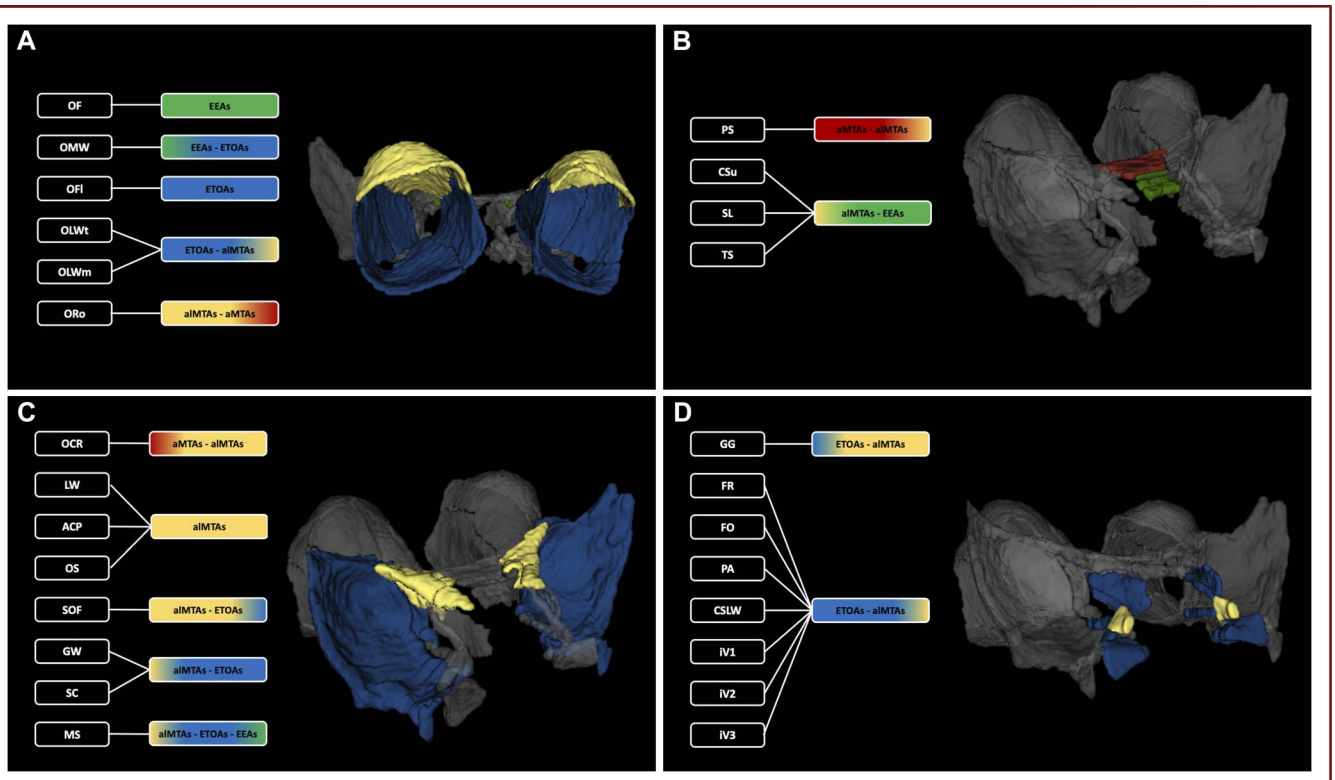


FIGURE 8. *Graphical summary of the best surgical approach for each anatomic target across the 4 macro-regions. 3-dimensional volume rendering intracranial views of the orbit and surrounding skull-base regions surfaces are shown bilaterally. Color coding identifies the approach providing the best exposure for each target: EEAs (green), ETOAs (blue), alMTAs (yellow), and aMTAs (red).* **A**, *Superolateral view of the orbit region: OF is better exposed by purely EEAs; OFl is better exposed by purely ETOAs; OMW, OLWt, and OLWm are better exposed by ETOAs; ORo is better exposed by alMTAs.* **B**, *Anterolateral view of the midline region: aMTAs allow better exposure of the PS; whereas EEAs provide better exposure of the CSu, SL, and TS.* **C**, *Anterolateral view of the spheno-orbital region: LW, ACP, and OS are better exposed by purely alMTAs; OCR and SOF are better exposed by alMTAs; GW, SC, and MS are better exposed by ETOAs.* **D**, *Anterolateral view of the CR: alMTAs allow better exposure of the GG, whereas ETOAs provide better exposure of the FR, FO, PA, CSLW, iV1, iV2, and iV3. ACP, anterior clinoid process; alMTAs, anterolateral microsurgical transcranial approaches; aMTAs, anterior microsurgical transcranial approaches; CR, cavernous region; CSLW, cavernous sinus lateral wall; CSu, chiasmatic sulcus; EEAs, endoscopic endonasal approaches; ETOAs, endoscopic transorbital approaches; FO, foramen ovale; FR, foramen rotundum; GG, gasserian ganglion; GW, greater wing; iV1, intracranial V1; iV2, intracranial V2; iV3, intracranial V3; LW, lesser wing; MS, maxillary strut; OCR, optic canal roof; OF, optic foramen; OFl, orbital floor; OLWm, orbit lateral wall (middle cranial fossa); OLWt, orbit lateral wall (temporal fossa); OMW, orbit medial wall; ORo, orbital roof; OS, optic strut; PA, petrous apex; PS, planum sphenoidale; SC, sagittal crest; SL, sphenoid limb; SOF, superior orbital fissure; TS, tuberculum sellae.*

orbital apex; our data show precisely where these routes rival or exceed transcranial corridors. For MR, our EETPA values align with reports from Kassam et al[38] and de Divitiis et al[34] on extended EEAs to the TS and PS but also highlight the residual advantages of ETBA for broad anterior skull-base exposure. Thus, rather than advocating a single "best" approach, our findings underscore the complementary nature of these corridors: EEAs for MR, ETOAs for lateral OR and anterior CR, and MTAs for panoramic SOR access and high-volume workspaces (Figures 8 and 9).

Clinically, spheno-orbital meningiomas are well suited for ETOAs, especially SETOA ± LO, due to ORo and OLW involvement and orbital decompression needs.[5,7,40,41] Meckel cave lesions, such as trigeminal schwannomas, may benefit from tailored anterolateral or combined transorbital-middle fossa approaches.[17,19] Cavernous sinus lesions require a compartment strategy, with EEAs addressing medial disease and ETOAs lateral and superior orbital extensions.[8,38,42] TS meningiomas remain an indication for EEAs, whereas MTAs are useful in selected complex cases.[34,42] Overall, approach selection should depend on lesion extension, consistent with region-based findings.

Limitations

This study is limited by its preclinical, cadaveric design. Pathological distortion (eg, tumor bulk, vascular engorgement, scar tissue) was not present, potentially underestimating the difficulty of real-world exposure. Cadaveric alcohol fixation with arterial silicone injection ensured stable anatomy and clear neurovascular landmarks but inevitably increased tissue stiffness. This may underestimate MTAs exposures. Likewise, interindividual variability in skull-base pneumatization and orbital geometry

© Congress of Neurological Surgeons 2026. Unauthorized reproduction of this article is prohibited.

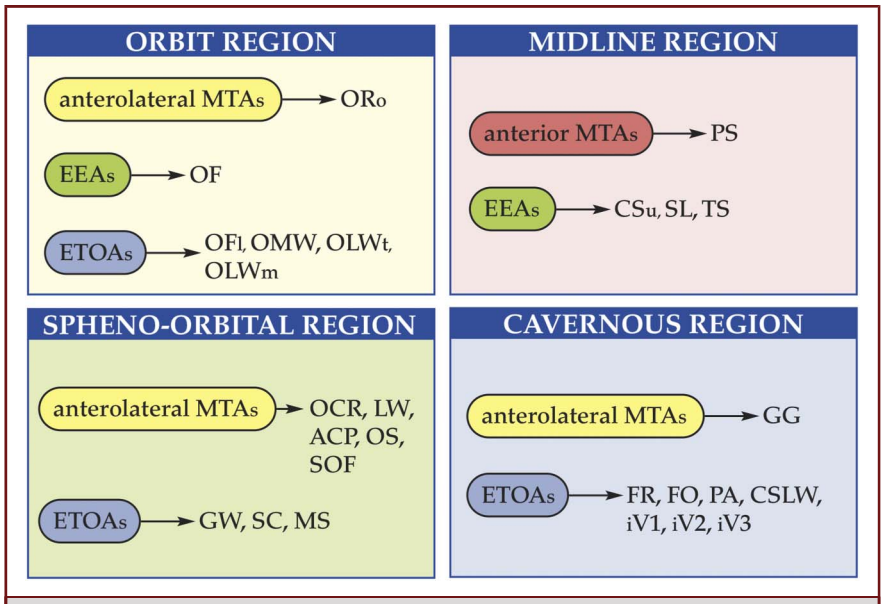


FIGURE 9. *Simplified conceptual schematic summarizing the best surgical corridors and their principal areas of exposure across the 4 analyzed macro-regions. Orbital region: ORo is better exposed through anterolateral MTAs; OF is better exposed through EEAs; OFl, OMW, OLWt, and OLWm are better exposed through ETOAs. Midline region: PS is better exposed through anterior MTAs; CSu, SL, and TS are better exposed through EEAs. Spheno-orbital region: OCR, LW, ACP, OS, and superior orbital fissure are better exposed through anterolateral MTAs; GW, SC, and MS are better exposed through ETOAs. cavernous region: GG is better exposed through anterolateral MTAs; FR, FO, PA, CSLW, iV1, iV2, and iV3 are better exposed through ETOAs. ACP, anterior clinoid process; CSLW, cavernous sinus lateral wall; CSu, chiasmatic sulcus; EEAs, endoscopic endonasal approaches; ETOAs, endoscopic transorbital approaches; FO, foramen ovale; FR, foramen rotundum; GG, gasserian ganglion; GW, greater wing; iV1, intracranial V1; iV2, intracranial V2; iV3, intracranial V3; LW, lesser wing; MS, maxillary strut; MTAs, microsurgical transcranial approaches; OCR, optic canal roof; OF, optic foramen; OFl, orbital floor; OLWm, orbit lateral wall (middle cranial fossa); OLWt, orbit lateral wall (temporal fossa); OMW, orbit medial wall; ORo, orbital roof; OS, optic strut; PA, petrous apex; PS, planum sphenoidale; SC, sagittal crest; SL, sphenoid limb; TS, tuberculum sellae.*

introduces unavoidable dispersion in measurements. Despite precautions, anatomic integrity may be affected in later dissections. Cadaveric models are static and do not reflect intraoperative dynamics. Brain relaxation techniques and pathology-related factors such as mass effect and edema may significantly alter working volumes. Therefore, measurements represent anatomic conditions rather than surgical simulation.

CONCLUSIONS

EEAs dominate midline access, ETOAs offer minimally invasive entry to the lateral orbit and anterior CS, and MTAs remain indispensable for panoramic SOR exposure and larger working volumes. Although preclinical, these findings offer practical, evidence-based guidance to optimize selection of the approach for complex orbital and skull-base surgery.

Funding

This study did not receive any funding or financial support.

Disclosures

The authors have no personal, financial, or institutional interest in any of the drugs, materials, or devices described in this article.

REFERENCES

1. Agosti E, Alexander AY, Plou P, et al. 360° around the orbit: key surgical anatomy of the microsurgical and endoscopic cranio-orbital and orbitocranial approaches. *Neurosurg Focus*. 2024;56(4):e2.
2. Ferrari M, Mattavelli D, Schreiber A, Nicolai P. Macroscopic and endoscopic anatomy of the anterior skull base and adjacent structures. *Adv Otorhinolaryngol*. 2020;84:1-12.
3. Salgado-López L, Campos-Leonel LCP, Pinheiro-Neto CD, Peris-Celda M. Orbital anatomy: anatomical relationships of surrounding structures. *J Neurol Surg B Skull Base*. 2020;81(4):333-347.
4. Rhoton AL. The orbit. *Neurosurgery*. 2002;51(4 Suppl):S303-S334.
5. Kong DS, Kim YH, Hong CK. Optimal indications and limitations of endoscopic transorbital superior eyelid surgery for spheno-orbital meningiomas. *J Neurosurg*. 2021;134(5):1472-1479.
6. Kong DS, Hong CK, Hong SD, et al. Selection of endoscopic or transcranial surgery for tuberculum sellae meningiomas according to specific anatomical features: a retrospective multicenter analysis (KOSEN-002). *J Neurosurg*. 2019;130(3):838-847.

© Congress of Neurological Surgeons 2026. Unauthorized reproduction of this article is prohibited.

7. Di Somma A, Andaluz N, Cavallo LM, et al. Endoscopic transorbital superior eyelid approach: anatomical study from a neurosurgical perspective. *J Neurosurg*. 2018;129(5):1203-1216.
8. Di Somma A, Cavallo LM, de Notaris M, et al. Endoscopic endonasal medial-to-lateral and transorbital lateral-to-medial optic nerve decompression: an anatomical study with surgical implications. *J Neurosurg*. 2017;127(1):199-208.
9. Di Somma A, Kong DS, de Notaris M, et al. Endoscopic transorbital surgery levels of difficulty. *J Neurosurg*. 2022;137(4):1187-1190.
10. Natori Y, Rhoton AL. Transcranial approach to the orbit: microsurgical anatomy. *J Neurosurg*. 1994;81(1):78-86.
11. Agosti E, Saraceno G, Rampinelli V, et al. Quantitative anatomic comparison of endoscopic transnasal and microsurgical transcranial approaches to the anterior cranial fossa. *Oper Neurosurg*. 2022;23(4):e256-e266.
12. Agosti E, Turri-Zanoni M, Saraceno G, et al. Quantitative anatomic comparison of microsurgical transcranial, endoscopic endonasal, and transorbital approaches to the spheno-orbital region. *Oper Neurosurg*. 2021;21(6):e494-e505.
13. Agosti E, Saraceno G, Qiu J, et al. Quantitative anatomical comparison of transnasal and transcranial approaches to the clivus. *Acta Neurochir (Wien)*. 2020;162(3):649-660.
14. Agosti E, De Maria L, Mattogno PP, et al. Quantitative anatomical studies in neurosurgery: a systematic and critical review of research methods. *Life (Basel)*. 2023;13(9):1822.
15. Alexander AY, Agosti E, Leonel LCPC, Lanzino G, Peris-Celda M. Comparison between the supracerebellar infratentorial and precuneal interhemispheric, transtentorial approaches to the cerebellomesencephalic fissure: an anatomoradiological study and illustrative cases. *Oper Neurosurg*. 2023;25(1):e6-e14.
16. Zanin L, Agosti E, Ebner F, et al. Quantitative anatomical comparison of surgical approaches to Meckel's cave. *J Clin Med*. 2023;12(21):6847.
17. Rampinelli V, Agosti E, Saraceno G, et al. Endoscopic subtemporal epidural keyhole approach: quantitative anatomic analysis of three surgical corridors. *World Neurosurg*. 2021;152:e128-e137.
18. Serioli S, Agosti E, Buffoli B, et al. Microsurgical transcranial approaches to the posterior surface of petrosal portion of the temporal bone: quantitative analysis of surgical volumes and exposed areas. *Neurosurg Rev*. 2023;46(1):48.
19. Saraceno G, Agosti E, Qiu J, et al. Quantitative anatomical comparison of anterior, anterolateral and lateral, microsurgical and endoscopic approaches to the middle cranial fossa. *World Neurosurg*. 2020;134:e682-e730.
20. Belotti F, Doglietto F, Schreiber A, et al. Modular classification of endoscopic endonasal transsphenoidal approaches to sellar region: anatomic quantitative study. *World Neurosurg*. 2018;109:e281-e291.
21. Doglietto F, Belotti F, Qiu J, et al. Endonasal and transoral approaches to the craniovertebral junction: a quantitative anatomical study. *Acta Neurochir Suppl*. 2019;125:37-44.
22. Doglietto F, Ferrari M, Mattavelli D, et al. Transnasal endoscopic and lateral approaches to the clivus: a quantitative anatomic study. *World Neurosurg*. 2018;113:e659-e671.
23. Schreiber A, Ferrari M, Rampinelli V, et al. Modular endoscopic medial maxillectomies: quantitative analysis of surgical exposure in a preclinical setting. *World Neurosurg*. 2017;100:44-55.
24. Ferrari M, Schreiber A, Mattavelli D, et al. Surgical anatomy of the parapharyngeal space: multiperspective, quantification-based study. *Head Neck*. 2019;41(3):642-656.
25. Ota HCU, Smith BG, Alamri A, et al. The IDEAL framework in neurosurgery: a bibliometric analysis. *Acta Neurochir (Wien)*. 2020;162(12):2939-2947.
26. Doglietto F, Qiu J, Ravichandiran M, et al. Quantitative comparison of cranial approaches in the anatomy laboratory: a neuronavigation based research method. *World J Methodol*. 2017;7(4):139-147.
27. Doglietto F, Radovanovic I, Ravichandiran M, et al. Quantification and comparison of neurosurgical approaches in the preclinical setting: literature review. *Neurosurg Rev*. 2016;39(3):357-368.
28. Jägersberg M, Brodard J, Qiu J, et al. Quantification of working volumes, exposure, and target-specific maneuverability of the pterional craniotomy and its minimally invasive variants. *World Neurosurg*. 2017;101:710-717.e2.
29. Perneczky A, Reisch R. *Keyhole Approaches in Neurosurgery: Volume 1: Concept and Surgical Technique*. Springer; 2009.
30. Spektor S, Valarezo J, Fliss DM, et al. Olfactory groove meningiomas from neurosurgical and ear, nose, and throat perspectives: approaches, techniques, and outcomes. *Neurosurgery*. 2005;57(4 Suppl):268-280.
31. Nakamura M, Struck M, Roser F, Vorkapic P, Samii M. Olfactory groove meningiomas: clinical outcome and recurrence rates after tumor removal through the frontolateral and bifrontal approach. *Neurosurgery*. 2007;60(5):844-852.
32. Ducic Y, Coimbra C. Minimally invasive transfrontal sinus approach to resection of large tumors of the subfrontal skull base. *Laryngoscope*. 2011;121(11):2290-2294.
33. Dehdashti AR, de Tribolet N. Frontobasal interhemispheric trans-lamina terminalis approach for suprasellar lesions. *Neurosurgery*. 2008;62(6 Suppl 3):1233-1239.
34. de Divitiis E, Esposito F, Cappabianca P, Cavallo LM, de Divitiis O. Tuberculum sellae meningiomas: high route or low route? A series of 51 consecutive cases. *Neurosurgery*. 2008;62(3):556-563.
35. Figueiredo EG, Deshmukh P, Nakaji P, et al. The minipterional craniotomy: technical description and anatomic assessment. *Neurosurgery*. 2007;61(5 Suppl 2):256-264.
36. Yaşargil MG. *Microneurosurgery*. Thieme; 1984.
37. van Furth WR, Agur AMR, Woolridge N, Cusimano MD. The orbitozygomatic approach. *Neurosurgery*. 2006;58(1 Suppl):ONS103-ONS107.
38. Kassam A, Snyderman CH, Mintz A, Gardner P, Carrau RL. Expanded endonasal approach: the rostrocaudal axis. Part I. Crista galli to the sella turcica. *Neurosurg Focus*. 2005;19(1):e3.
39. Ferrari M, Schreiber A, Mattavelli D, et al. The inferolateral transorbital endoscopic approach: a preclinical anatomic study. *World Neurosurg*. 2016;90:403-413.
40. Locatelli D, Restelli F, Alfiero T, et al. The role of the transorbital superior eyelid approach in the management of selected spheno-orbital meningiomas: in-depth analysis of indications, technique, and outcomes from the study of a cohort of 35 patients. *J Neurol Surg B Skull Base*. 2022;83(2):145-158.
41. Agosti E, Zeppieri M, De Maria L, et al. Surgical treatment of spheno-orbital meningiomas: a systematic review and meta-analysis of surgical techniques and outcomes. *J Clin Med*. 2023;12(18):5840.
42. Mastantuoni C, Cavallo LM, Esposito F, et al. Midline skull base meningiomas: transcranial and endonasal perspectives. *Cancers (Basel)*. 2022;14(12):2878.
43. Kong DS, Young SM, Hong CK, et al. Clinical and ophthalmological outcome of endoscopic transorbital surgery for cranioorbital tumors. *J Neurosurg*. 2019;131(3):667-675.
44. Bhuskute GS, Gosal JS, Alsavaf MB, et al. Endoscopic precaruncular medial transorbital and endonasal multiport approaches to the contralateral skull base: a clinicoanatomical study. *Neurosurg Focus*. 2024;56(4):e10.
45. Kim JH, Hong CK, Shin HJ, Kong DS. Feasibility and efficacy of endoscopic transorbital optic canal decompression for meningiomas causing compressive optic neuropathy. *J Neurosurg*. 2024;140(2):412-419.

Acknowledgments

The authors offer special thanks to the Anatomy Laboratory "Luigi Fabrizio Rodella", Department of Clinical and Experimental Sciences, Section of Anatomy and Physiopathology, University of Brescia, Brescia, Italy. Author contributions: Conceptualization, E.A., M.M.F., and F.D.; methodology, E.A., M.M.F., P.P.P., M.R., M.P.-C., L.A., A.Y.A., B.B., K.M., and F.D.; validation, E.A., M.V., P.P.P., L.A., L.H., R.R., M.T.-Z., K.M., M.M.F., and F.D.; formal analysis, E.A., A.Y.A., L.A., K.M., and M.V.; investigation, E.A., M.V., K.M., P.P.P., L.A., M.M.F., and F.D.; resources, E.A., M.R., L.A., P.P.P., V.R., B.B., L.H., R.R., M.T.-Z., K.M., M.M.F., and F.D.; data curation, E.A., M.R., L.A., K.M., V.R., and M.V.; writing-original draft preparation, E.A. and M.V.; writing-review and editing, E.A., K.M., and M.V.; visualization, all authors; supervision, E.A., B.B., M.P.-C., M.M.F., and F.D.; project administration, E.A., M.M.F., and F.D. All authors have read and agreed to the published version of the manuscript.

Supplemental digital content *is available for this article at operativeneurosurgery-online.com.*

Supplementary Digital Content 1: Table 1. Comparison of surgical exposure for the optic foramen. **Table 2.** Comparison of surgical exposure for the orbit lateral wall (middle cranial fossa). **Table 3.** Comparison of surgical exposure for the orbit lateral wall (temporal fossa). **Table 4.** Comparison of surgical exposure for the orbit medial wall. **Table 5.** Comparison of surgical exposure for the orbital floor. **Table 6.** Comparison of surgical exposure for the orbital roof. **Table 7.**

© Congress of Neurological Surgeons 2026. Unauthorized reproduction of this article is prohibited.

Comparison of surgical exposure for the chiasmatic sulcus. **Table 8.** Comparison of surgical exposure for the planum sphenoidale. **Table 9.** Comparison of surgical exposure for the sphenoid limb. **Table 10.** Comparison of surgical exposure for the tuberculum sellae. **Table 11.** Comparison of surgical exposure for the anterior clinoid process. **Table 12.** Comparison of surgical exposure for the greater wing. **Table 13.** Comparison of surgical exposure for the lesser wing. **Table 14.** Comparison of surgical exposure for the maxillary strut. **Table 15.** Comparison of surgical exposure for the optic canal roof. **Table 16.** Comparison of surgical exposure for the optic strut. **Table 17.** Comparison of surgical exposure for the sagittal crest. **Table 18.** Comparison of surgical exposure for the superior orbital fissure. **Table 19.** Comparison of surgical exposure for the foramen ovale. **Table 20.** Comparison of surgical exposure for the cavernous sinus, lateral wall. **Table 21.** Comparison of surgical exposure for the foramen rotundum. **Table 22.** Comparison of surgical exposure for the gasserian ganglion. **Table 23.** Comparison of surgical exposure for the intracranial V1. **Table 24.** Comparison of surgical exposure for the intracranial V2. **Table 25.** Comparison of surgical exposure for the intracranial V3. **Table 26.** Comparison of surgical exposure for the petrous apex. **Table 27.** Table indicating the average, minimum, maximum, and standard deviation values of the noncrossing volume of each simulated approach in cm^3.

© Congress of Neurological Surgeons 2026. Unauthorized reproduction of this article is prohibited.